Pergamon

Int. J. Solids Structures Vol. 31, No. 18, pp. 2519–2536, 1994

0020–7683/94 $7.00 + .00

0020-7683(94)E0039-X

A MECHANICS MODEL FOR THE COMPRESSIVE RESPONSE OF FIBER REINFORCED COMPOSITES

I. CHUNG and Y. WEITSMAN†
Department of Engineering Science and Mechanics, The University of Tennessee at Knoxville, Tennessee, U.S.A.

(*Received* 17 *May* 1993; *in revised form* 25 *January* 1994)

Abstract—This article presents a model for the uni-axial compressive response of uni-directionally reinforced fibrous composite. The model accounts for the non-linear shear response and the failure strain of the matrix, incorporating both aspects into a non-linear field equation which governs the load-deflection process. In addition, the model considers the effects of two kinds of geometric imperfections, namely, initial fiber waviness and random fiber spacing. It is shown that, under uni-axial compression, random fiber spacing may instigate the formation of severe transverse loadings on the fibers, which suggest the existence of a transitional mechanism from micro-buckling to micro-kinking.

Computational results are presented which illuminate the effects of several material and geometric factors on the compressive strength of composites.

1. INTRODUCTION

The compressive behavior of composite materials has been studied extensively during the past three decades and a review of literature on the subject is beyond the scope of this paper. Substantial listings of references on the subject can be found in the articles by Shuart (1985), Camponeschi (1991), Guynn *et al.* (1992) and Piggott (1993). Suffice it to say that the compressive response of composites was found to depend on the properties and response of the constituent materials and on the fiber volume fraction. As may be expected, compressive strength is sensitive to imperfections.

The essential novel feature in the present work is the incorporation of random fiber spacings, as commonly encountered in composites, into a model for their compressive behavior. The main consequence of the foregoing feature is that it predicts a response which involves the emergence of highly concentrated lateral forces on the fibers simultaneously with micro-buckling. These lateral forces are a most likely cause for the development of kinks. One of the outstanding issues regarding the compressive response of composites is that the common methodology for predicting compressive failure stems from considerations of buckling and stability, while most failed specimens exhibit localized kink bands which span the thicknesses of the test coupons. It seems that all other models address micro-buckling and micro-kinking exclusively of each other, and can thus be grouped accordingly.

(1) *Models which consider buckling*

These include the work of Rosen (1965), which seems to be the first article on compressive failure of composites. Considering "shear-mode buckling", that model predicted a failure stress $\sigma_{CR} = G_m/(1-V_f)$, where G_m is the shear modulus of the matrix and V_f the fiber volume fraction. That prediction is inadequate for two reasons: (a) it gives σ_{CR} which is several times higher than experimental values; (b) the relation $\sigma_{CR} \sim 1/(1-V_f)$ contradicts experimental observations which show that σ_{CR} grows linearly with V_f (at least up to $V_f \approx 0.55$) [e.g. Piggott and Harris (1980); Morley (1987)].

Several modifications to Rosen's model were introduced subsequently. Primarily, these modifications considered non-linear shear response of the matrix and initial fiber waviness [e.g. Wang (1978); Lin and Zhang (1992); Guynn *et al.* (1992); Highsmith *et al.* (1992)

† Also at Engineering Technology Division, Oak Ridge National Laboratory, Tennessee, U.S.A.

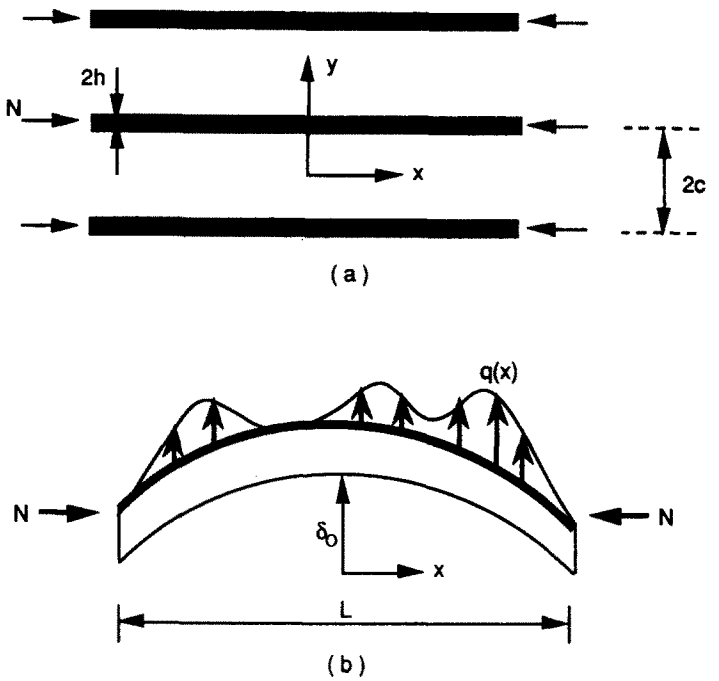

Fig. 1. (a) A fiber composite modelled as a two dimensional lamellar region consisting of fiber and matrix plates, (b) a deformed single cell.

and others listed in the aforementioned review articles]. Additional modifications included the incorporation of fibers' shear-deformation, such as by Davis (1975), or the accounting for large deformations of the fibers by Yin (1992). Though the latter model stems from a buckling formulation, it is worth noting that it proposes a criterion for kink formation, which occurs when fibers' curvature attains a critical value.

(2) *Models which consider the* a priori *existence of kinks*

These include works by Evans and Adler (1978), Hahn and Williams (1986) and Budiansky and Fleck (1992).

The compressive response of multi-directionally reinforced laminates such as Shuart (1989), and of cylindrical shells such as Blake and Starbuck (1993), is beyond the scope of this article. These complex circumstances activate various modes of failure which do not occur in the uni-directional case considered herein.

In all the above works, the fiber reinforced composites were viewed as lamellar regions which consist of fiber and matrix layers as shown in Fig. 1(a). It should be noted that several investigators (Sadowsky *et al.*, 1967; Hermann *et al.*, 1967; Lanir and Fung, 1972; Greszczuk, 1975) considered fibers of cylindrical geometry. All those works assumed linear elastic behavior of fiber and matrix materials.

In addition to random fiber spacing, the current model includes initial fiber waviness and considers the non-linear shear stress–strain response in the matrix. The fibers are assumed to deform in accordance with classical beam theory.

2. FORMULATION AND RESULTS

Consider a uni-axially reinforced composite which, following Rosen (1965), is represented by a two-dimensional layered array as shown in Fig. 1(a). Let x and y denote Cartesian coordinates in directions parallel and transverse to the layers, and designate by $2h$ the thickness of a "fiber layer" centered within a composite layer of thickness $2c$. Consequently we have $V_f = h/c$ and $V_m = (c-h)/c$, where V_f and V_m are fiber and matrix volume fractions, respectively.

We focus attention on the "shear mode" of buckling (Rosen, 1965; Garg *et al.*, 1973), where all fibers buckle in phase. Then, following Rosen's premises (1965) for high performance composite material systems, we assume that the external compressive load N is borne entirely by the fiber region, which is modelled as a Bernoulli–Euler beam, while the matrix responds in shear only. Consequently, we have the following familiar expression for γ_{xy}^{m}, the shear strain in the matrix:

$$\gamma_{xy}^{m} = \frac{1}{1-V_f}\frac{dv^f}{dx}. \tag{1}$$

In eqn (1), v^f denotes the lateral displacement (in the y-direction) of the fiber. In view of the assumption of Bernoulli–Euler theory, v^f, and thereby also γ_{xy}^{m}, depends only on x.

In addition, we consider a micro-buckling length L and initial fiber waviness $v_0^f(x)$ with periodicity of $2L$. In the sequel, we let $v_0^f(x) = \delta_0 \cos(\pi x/L)$, though this specific choice is not essential to our method. Finally, in anticipation of the circumstances which emerge due to non-uniform fiber spacings, we denote by $q(x)$ the distributed lateral load on the fiber [see Fig. 1(b)].

Considering non-linear shear response of the matrix, we write

$$\tau_{xy}^{m} = G_e^m F(\gamma_{xy}^{m}), \tag{2}$$

where the function $F(\gamma_{xy}^{m})$ expresses that non-linear shear behavior of the matrix scaled by the initial shear modulus G_e^m.

The longitudinal strain in the fiber, ε_x^f, under the combined effects of compression and bending is given by

$$\varepsilon_x^f = \frac{du^f}{dx} + \frac{1}{2}\left[\left(\frac{dv^f}{dx}+\frac{dv_0^f}{dx}\right)^2 - \left(\frac{dv_0^f}{dx}\right)^2\right] - y\frac{d^2v^f}{dx^2}. \tag{3}$$

In eqn (3), u^f denotes the fiber displacement in the direction of x.

Consequently, the axial displacement at $x = L/2$ is given by

$$u_{x=L/2}^f = \Delta = \frac{1}{2}\int_0^{L/2}\left[\left(\frac{dv^f}{dx}+\frac{dv_0^f}{dx}\right)^2 - \left(\frac{dv_0^f}{dx}\right)^2\right]dx + \frac{1}{2}\frac{NL}{EA}. \tag{4}$$

As can be noted from eqns (3) and (4), the hypothesis that fibers deform in-phase implies that u^f and v^f are common to all fibers regardless of their spacing. On the other hand, eqns (1) and (2) state that the support provided by the matrix varies with the fiber volume fraction V_f. These observations imply the existence of lateral loads, $q = q(x)$, which enforce a common, in-phase deformation of all fibers in the case of non-uniform spacing. To emphasize their dependence of the spacing c, we shall write $q = q(x, c)$.

Consider an individual cell of width $2c$. The principle of virtual work yields

$$\int_{V^f}\sigma_x^f\delta\varepsilon_x^f\,dV^f + \int_{V^m}\tau_{xy}^{m}\delta\gamma_{xy}^{m}\,dV^m - \int_0^{L/2} q(x,c)\delta v^f dx + N\delta\Delta = 0. \tag{5}$$

Substitution of expressions (1)–(4) into eqn (5) and employment of integrations by parts yield the following field equation and boundary conditions for each individual cell:

$$EI_f\frac{d^4v^f}{dx^4} - 2cG_e^m\frac{d}{dx}F\left(\frac{1}{1-V_f}\frac{dv^f}{dx}\right) + N\left(\frac{d^2v^f}{dx^2}+\frac{d^2v_0^f}{dx^2}\right) = q(x,c), \tag{6}$$

with

$$\frac{dv^f}{dx} = 0, \quad \frac{d^3v^f}{dx^3} = 0 \quad \text{at} \quad x = 0$$

$$v^f = 0, \quad \frac{d^2v^f}{dx^2} = 0 \quad \text{at} \quad x = \frac{L}{2}. \tag{7}$$

Note that, in view of the non-linearity of F in its argument, eqn (6) is a non-linear differential equation for v^f.

Turning to the case of random fiber spacing, let $p(c)$ denote the probability density of the cell dimension $2c$. Obviously

$$\int_h^\infty p(c)\,dc = 1. \tag{8}$$

In the present circumstance the principle of virtual work gives

$$\int_h^\infty p(c)\left\{\int_{V^f} \sigma_x^f \delta\varepsilon_x^f\,dV^f + \int_{V^m} \tau_{xy}^m \delta\gamma_{xy}^m\,dV^m - \int_0^{L/2} q(x,c)\delta v^f\,dx + N\delta\Delta\right\}dc = 0. \tag{9}$$

Furthermore, in the absence of external lateral loads, equilibrium in the direction of y requires

$$\int_h^\infty p(c)\left(\int_0^{L/2} q(x,c)\,dx\right)dc = 0. \tag{10}$$

Integration-by-parts of eqn (9), upon expressing all variations in terms of $\delta(dv^f/dx)$, gives the following field equation for v^f:

$$EI_f\frac{d^3v^f}{dx^3} - \int_h^\infty 2cp(c)G_e^m\frac{d}{dx}F\left(\frac{1}{1-V_f}\frac{dv^f}{dx}\right)dc + N\left(\frac{dv^f}{dx} + \frac{dv_0^f}{dx}\right) = 0. \tag{11}$$

The boundary conditions for the case of randomly spaced fiber remain the same as those given in eqns (7).†

It is advantageous to further reduce the order of the differential equation given in eqn (11) and express it in a non-dimensional form in terms of the following non-dimensional parameters:

$$X = \frac{x}{L}, \quad Y = \frac{dv^f}{dx}, \quad \varepsilon = \frac{\delta_0}{L}. \tag{12}$$

In addition, the probability distribution function $p(c)$ can be converted to a probability distribution function $\hat{p}(V_f)$.

In view of expression (12), the non-dimensional form of eqn (11) reads

$$\frac{d^2Y}{dX^2} - \int_0^1 \hat{p}(V_f)\alpha^2(1-V_f)F\left(\frac{Y}{1-V_f}\right)dV_f + \lambda^2 Y = -\lambda^2 Y_0, \tag{13}$$

where

† In view of eqn (10), it was possible to derive differential eqn (11) which is one order lower than that given in eqn (6). The lower order eqn (11) enables the determination of the lateral displacement v^f to within a rigid translation, which is of no relevance to the failure mechanisms considered in this work. An additional integration of expression (11) with respect to x, further reduces the order of the differential equation, leading to a solution which incorporates an indeterminate rigid body rotation.

$$\alpha^2 = \frac{2h}{V_f(1-V_f)}\frac{G_e^m L^2}{EI_f}, \quad \lambda^2 = \frac{NL^2}{EI_f}, \quad Y_0 = -\varepsilon\pi \sin \pi X. \tag{14}$$

The boundary conditions which accompany the second order non-linear differential eqn (13) are

$$Y(0) = 0, \quad \frac{dY}{dX}\left(\frac{1}{2}\right) = 0. \tag{15}$$

In the case of uniform fiber spacing, eqn (13) reduces to

$$\frac{d^2Y}{dX^2} - \alpha^2(1-V_f)F\left(\frac{Y}{1-V_f}\right) + \lambda^2 Y = -\lambda^2 Y_0. \tag{16}$$

Note that for the linearly elastic case with uniformly spaced fibers, $F(Y/(1-V_f)) = Y/(1-V_f)$ and eqn (16) takes the simple form

$$\frac{d^2Y}{dX^2} - \alpha^2 Y + \lambda^2 Y = -\lambda^2 Y_0,$$

with the solution

$$Y = \frac{\varepsilon\pi\lambda^2}{\lambda^2 - \pi^2 - \alpha^2} \sin \pi X.$$

This corresponds to the buckling load predicted by Rosen (1965), namely $\lambda^2 = \pi^2 + \alpha^2$. Note that the above result assumed that the magnitude of the linearly elastic shear strain in the matrix is not limited by any ultimate or plastic level.

However, if one considers a linearly elastic matrix response followed by an ideally plastic deformation at $\gamma_{xy}^m = \gamma_p$, then plastic yield begins at $X = 1/2$ and the onset of plastic deformation is found to occur at

$$\lambda^2 = \frac{(\pi^2+\alpha^2)(1-V_f)\gamma_p}{\varepsilon\pi + (1-V_f)\gamma_p} = \lambda^2(\gamma_p). \tag{17}$$

The above result agrees with the value obtained by Steif (1988) for the slippage initiation load, beyond which the matrix no longer supports the deformed fibers.

Case 1. *Uniformly spaced fibers with bi-linear shear modulus of the matrix*

Consider a bi-linear shear stress–strain response of the matrix material, given by the following expression for $F(\gamma_{xy}^m)$

$$G_e^m F(\gamma_{xy}) = \begin{cases} G_p^m(\gamma_{xy} - \gamma_y) + G_e^m \gamma_y & \text{if} \quad \gamma_{xy} > \gamma_y \\ G_e^m \gamma_{xy} & \text{if} \quad -\gamma_y < \gamma_{xy} < \gamma_y \\ G_p^m(\gamma_{xy} + \gamma_y) - G_e^m \gamma_y & \text{if} \quad \gamma_{xy} < -\gamma_y \end{cases}. \tag{18}$$

In eqn (18), γ_y is the strain level where the slope of the bi-linear stress–strain diagram changes from an initial value G_e^m to the strain hardening value G_p^m. It will be shown in this section that the buckling associated with the response expressed in eqns (18) can be handled analytically.

For loads that correspond to λ^2 which exceeds $\lambda^2(\gamma_y)$ in eqn (18), the shear response of the matrix will follow the bi-linear stress–strain relation over a region $\xi < X < 1/2$, but

will still remain linearly elastic within the central region $0 < X < \xi$. Obviously ξ decreases with increasing λ^2. Substitution of expressions (18) into eqn (16) gives

$$\frac{d^2Y}{dX^2} - \alpha_e^2 Y + \lambda^2 Y = -\lambda^2 Y_0 \qquad \text{at} \quad 0 < X < \xi$$

$$\frac{d^2Y}{dX^2} - \alpha_p^2 Y + \lambda^2 Y = -\lambda^2 Y_0 - \beta^2 \quad \text{at} \quad \xi < X < \tfrac{1}{2}, \tag{19}$$

where α_e and α_p are defined according to eqn (14) with shear moduli G_e^m and G_p^m, respectively, and

$$\beta^2 = \frac{2h}{V_f(1-V_f)} \frac{(G_e^m - G_p^m)L^2}{EI_f} \gamma_y.$$

The boundary and continuity conditions associated with eqns (19) are

$$\frac{dY}{dX}\left(\frac{1}{2}\right) = 0, \quad Y(0) = 0, \quad Y(\xi^+) = Y(\xi^-), \quad \frac{dY}{dX}(\xi^+) = \frac{dY}{dX}(\xi^-), \quad Y(\xi) = -V_m \gamma_y. \tag{20}$$

The above conditions correspond, respectively, to the vanishing of the moment at $x = L/2$, and of the shear at $x = 0$, the continuity of shear and moment at $x = \xi L$ and the requirement that, by hypothesis, $|\gamma_{xy}^m| = \gamma_y$ at $x = \xi L$. The five conditions given in eqn (20) determine the four unknowns associated with the two second order differential equations (19), as well as the yet unknown location ξ.

Note that the solution for Y determines the displacement v^f to within arbitrary rigid translations and rotations, which are determined from the requirement of continuity of v^f and dv^f/dx at $x = \xi L$, as well as $v^f(0) = 0$ and $dv^f/dx = 0$ at $x = L/2$.

The solution to eqns (19) reads:

for $0 < X < \xi$

$$Y_-(X) = -\frac{\sinh \kappa_e X}{\sinh \kappa_e \xi}\left\{\frac{\varepsilon\pi\lambda^2}{\lambda^2 - \pi^2 - \alpha_e^2}\sin \pi\xi + (1-V_f)\gamma_y\right\} + \frac{\varepsilon\pi\lambda^2}{\lambda^2 - \pi^2 - \alpha_e^2}\sin \pi X; \tag{21}$$

for $\xi < X < 1/2$ and $\lambda^2 < \alpha_p^2$

$$Y_+(X) = -\frac{\cos \kappa_p(1-2X)/2}{\cos \kappa_p(1-2\xi)/2}\left\{\frac{\varepsilon\pi\lambda^2}{\lambda^2 - \pi^2 - \alpha_p^2}\sin \pi\xi + (1-V_f)\gamma_y - \frac{\beta^2}{\lambda^2 - \alpha_p^2}\right\}$$
$$+ \frac{\varepsilon\pi\lambda^2}{\lambda^2 - \pi^2 - \alpha_p^2}\sin \pi X - \frac{\beta^2}{\lambda^2 - \alpha_p^2}; \tag{22a}$$

for $\xi < X < 1/2$ and $\lambda^2 > \alpha_p^2$

$$Y_+(X) = -\frac{\cosh \kappa_p(1-2X)/2}{\cosh \kappa_p(1-2\xi)/2}\left\{\frac{\varepsilon\pi\lambda^2}{\lambda^2 - \pi^2 - \alpha_p^2}\sin \pi\xi + (1-V_f)\gamma_y - \frac{\beta^2}{\lambda^2 - \alpha_p^2}\right\}$$
$$+ \frac{\varepsilon\pi\lambda^2}{\lambda^2 - \pi^2 - \alpha_p^2}\sin \pi X - \frac{\beta^2}{\lambda^2 - \alpha_p^2}. \tag{22b}$$

In the above equations, $\kappa_e = \sqrt{\alpha_e^2 - \lambda^2}$ and $\kappa_p = \sqrt{|\alpha_p^2 - \lambda^2|}$.

Equations (21) and (22) match all the conditions (20) except the continuity $dY/dX(\xi^+) = dY/dX(\xi^-)$. The latter condition yields a characteristic equation, upon

differentiation of eqns (21) and (22), which relates the position of ξ to the load parameter λ^2. This characteristic equation must be solved numerically, with the physically meaningful solution corresponding to the lowest value of λ^2.

In our computations we utilized the constituent properties reported by Guynn *et al.* (1992) for AS4/PEEK at 21°C. Accordingly, we took $E_f = 67$ GPa, $L = 330$ μm and $\delta_0 = 1.65$ μm and $V_f = 0.6$. For purposes of comparison we also considered additional values of V_f in the sequel. The non-linear shear stress–strain response was approximated by a bi-linear relationship with $G_e^m = 1.3$ GPa, $G_p^m = 0.33$ GPa and $\gamma_y = 4.2\%$.

The resulting stress-deflection curves are shown in Fig. 2 for various values of V_f. The symbols "+" on those curves correspond to load and displacement values at onset of departure from linearity in the shear stress–strain response of the matrix. Such departure occurs when $|\gamma_{xy}^m| = \gamma_y$ at $X = 1/2$. Note that when $V_f = 0.9$ the composite can carry compressive loads which exceed the level which cause departure from linear matrix response. However, for $V_f = 0.3$ and $V_f = 0.6$, the stress-deflection curves exhibit the so called "finite disturbance buckling behavior" resembling the buckling of cylindrical shells under uni-axial compression or spherical shells under external pressure (Simitses, 1976). It is interesting to note that for $V_f = 0.3$ and $V_f = 0.6$ the cusps in the stress-deflection curves, which correspond to maximal load levels prior to buckling, occur at magnitudes just above those which cause $|\gamma_{xy}^m| = \gamma_y$ at $X = 1/2$. It is obvious that the theoretically predicted cusps for $V_f = 0.3$ and 0.6 cannot be realized experimentally. Under load controlled tests the maximal loads will be followed by total collapse and under displacement controlled circumstances the specimen would snap through to the lower load levels along the vertical dashed lines shown in Fig. 2.

Further insight into the compressive response predicted by the solution to eqns (19) and (20) is provided in Figs 3 and 4. The dimensionless length $\hat{\xi}(\hat{\xi} = 1/2 - \xi)$ of the regions where the matrix shear strain $|\gamma_{xy}^m|$ exceeds the linear elastic limit γ_y is plotted vs the applied compressive stress σ_c in Fig. 3 for fiber volume fractions $V_f = 0.3$, 0.6 and 0.9. Note that σ_c increases monotonically with $\hat{\xi}$ for $V_f = 0.9$, but decreases (after very slight initial amplifications) for $V_f = 0.3$ and 0.6.

The variation of the matrix shear strain γ_{xy}^m with the dimensionless distance X along the fiber/matrix interfaces is shown in Fig. 4 for $V_f = 0.6$. The four curves in that figure correspond to distinct levels of non-dimensional load λ. The top curve, with $\lambda = 23.10$ represents typical linear elastic results, with $|\gamma_{xy}^m| < \gamma_y$ for all X and thereby also $\hat{\xi} = 0$. In this case we obtain a sinusoidal variation of γ_{xy}^m which agrees with earlier results (Wang, 1978; Lin and Zhang, 1992), namely $\gamma_{xy}^m = A \sin \pi X$ with $A = \varepsilon\pi\lambda^2/[(1 - V_f)(\lambda^2 - \pi^2 - \alpha^2)]$. The foregoing sinusoidal variation persists until the onset of inelastic response at $X = 1/2$ which occurs at $\lambda = \lambda_y = 30.79$. This result is shown by the dashed line in Fig. 4. The maximal value of the compressive load, associated with $\lambda = \lambda_{max} = 30.81$, corresponds to an inelastic zone of dimensionless length $\hat{\xi} = 0.05$. In this case the variation of γ_{xy}^m with X,

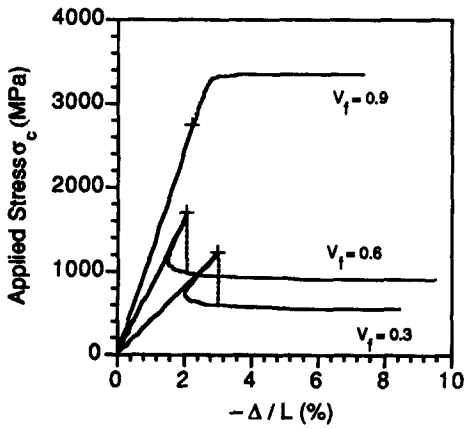

Fig. 2. The scaled compressive displacement Δ/L at $X = 0.5$ vs applied compressive stress σ_c for various fiber volume fractions V_f (symbol "+" corresponds to the circumstance of $|\gamma_{xy}^m(X = \frac{1}{2})| = \gamma_y$).

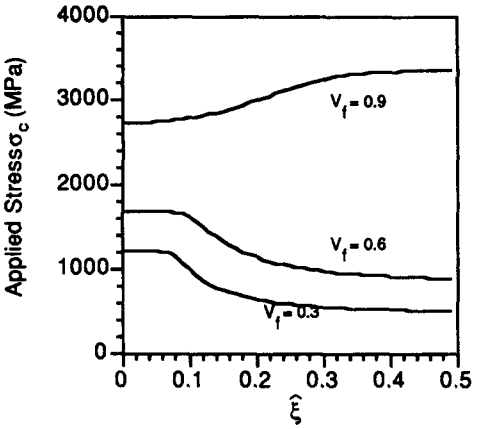

Fig. 3. The dimensionless length, $\hat{\xi} = 0.5 - \xi$, of the inelastic zone of matrix shear response $[|\gamma_{xy}^m| > \gamma_y$ in eqn (18)] vs applied compressive stress for $V_f = 0.3$, 0.6 and 0.9.

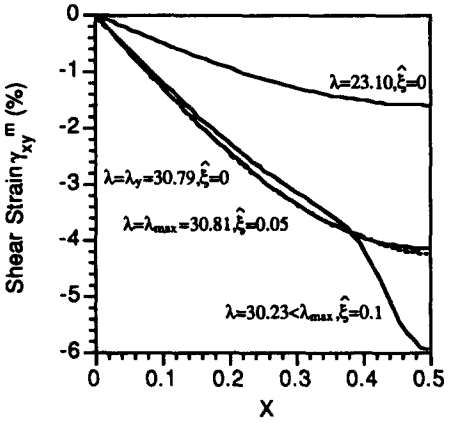

Fig. 4. The variation of the matrix shear strain γ_{xy}^m vs the non-dimensionalized distance X along the fiber/matrix interface at several values of non-dimensionalized applied compressive stress λ. Fiber volume fraction $V_f = 0.6$. Onset of departure from linear elastic matrix shear response at $\lambda = \lambda_y = 30.79$, maximum compressive stress at $\lambda = \lambda_{max} = 30.81$.

shown by the dotted line in Fig. 4, is no longer sinusoidal. Beyond $\hat{\xi} = 0.05$, values of λ decrease while Δ/L increase according to Fig. 2. A typical circumstance, corresponding to $\hat{\xi} = 0.1$ and $\lambda = 30.23$, is shown by the solid line in Fig. 4.

Case 2. Non-uniformly spaced fibers

Statistical consideration of cell size distributions. As noted in the Introduction, non-uniformity in fiber spacing introduces a new aspect into the compressive and buckling behavior of fiber reinforced composites, namely transverse internal lateral loads associated with the common deformation of the fibers. Following the statistics of spatially distributed data and the concept of Voronoi cell tessellation, as employed to represent the spatial distribution of spherical and cylindrical inclusions (Davy and Guild, 1988), we assume a cumulative distribution function for the cell size $2c$ described by a Poisson's point process

$$P(C > c) = \exp(-2\mu c). \tag{23}$$

In eqn (23), μ is the frequency of Voronoi cells in a unit length, with a mean cell size of μ^{-1}. The above consideration is subject to the restriction that fiber regions cannot overlap, namely $c > h$ ("Gibbs hard core process"). Therefore, eqn (23) is modified to read

$$P(C > c) = \exp[-2\mu'(c-h)]. \tag{24}$$

Since μ^{-1} is still the expected value of the Voronoi cell size, namely

$$\mu^{-1} = E(2c) = -\int_h^\infty 2c \frac{\mathrm{d}}{\mathrm{d}c} P(C > c)\,\mathrm{d}c,$$

one obtains

$$\mu' = \frac{\mu}{1-2\mu h}. \tag{25}$$

Equations (23)–(25) can be expressed in terms of the fiber volume fraction V_f, as employed in eqn (13). Let $\bar{V}_f$ denote the average ("nominal") value of the fiber volume fraction and $2\bar{c} = \mu^{-1}$ the average length of the Voronoi cells, then $\bar{V}_f = h/\bar{c} = 2h\mu$. Consequently, we have

$$\mu' = \frac{\bar{V}_f}{2h(1-\bar{V}_f)}$$

and

$$P(C > c) = \exp\left[-\frac{\bar{V}_f}{1-\bar{V}_f}\left(\frac{c}{h}-1\right)\right].$$

Therefore, the cumulative probability that the fiber volume fraction $\tilde{V}_f$ exceeds a value V_f is

$$\hat{P}(\tilde{V}_f > V_f) = 1-P(C > c) = 1-\exp\left[-\frac{\bar{V}_f}{1-\bar{V}_f}\left(\frac{1}{V_f}-1\right)\right]. \tag{26}$$

The probability density distribution which corresponds to eqn (26) is

$$\hat{p}(V_f) = -\frac{\mathrm{d}}{\mathrm{d}V_f}\hat{P}(\tilde{V}_f > V_f) = \frac{\bar{V}_f}{1-\bar{V}_f}\frac{1}{V_f^2}\exp\left[-\frac{\bar{V}_f}{1-\bar{V}_f}\left(\frac{1}{V_f}-1\right)\right]. \tag{27}$$

Computational results for $\hat{p}(V_f)$ vs V_f are shown in Fig. 5 for three nominal (average) values of $\bar{V}_f$ ($\bar{V}_f = 0.3$, 0.6 and 0.9).

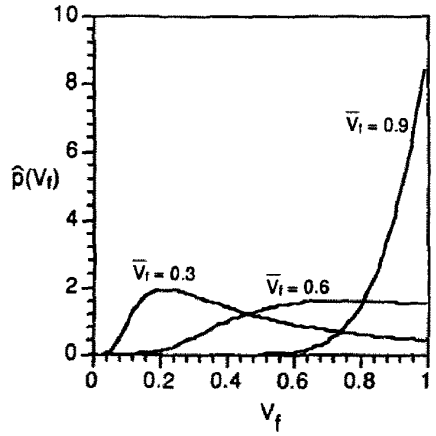

Fig. 5. Distribution of local fiber volume fraction for randomly spaced fiber composites with average fiber volume fraction $\bar{V}_f$ of 0.3, 0.6 and 0.9.

The compressive response with randomly spaced fibers

The probability density $\hat{p}(V_f)$ given in eqn (27) was incorporated into the formulation expressed in eqns (11) and (13) and employed to predict the compressive response of Gr/PEEK (APC-2) composite with $\bar{V}_f = 0.6$ at a temperature of $T = 21°C$. Based upon the data of Guynn *et al.* (1992), the non-linear shear behavior of the PEEK resin was fitted by a Ramberg–Osgood expression

$$\gamma_{xy}^m = \frac{\tau_{xy}^m}{G_e^m} + \left(\frac{\tau_{xy}^m}{A}\right)^{1/n}, \tag{28}$$

where $G_e^m = 1.3$ GPa as in the previous section, $A = 94.4$ MPa and $n = 0.12$. In addition, we took $\varepsilon = \delta_0 L = 1/200$ as before and assumed, somewhat arbitrarily, resin failure to occur at $\gamma_{xy}^m = \gamma_u = 10\%$. The latter assumption was guided by the observed tensile failure at $\varepsilon_u \sim 4$–5% for PEEK at room temperature reported by Johnston *et al.* (1991). The shear stress–strain response considered in the foregoing representation is shown in Fig. 6.

The solution to eqn (13), with $Y(0) = 0$, $dY/dX(1/2) = 0$ together with eqns (27) and (28), was obtained numerically. Note that eqn (28) was supplemented by $\tau_{xy}^m = 0$ for $|\gamma_{xy}^m| > \gamma_u$. To implement the numerical solution, the field eqn (13) was expressed by finite differences as given by Na (1979), and solved iteratively by a quasi-linearization method.

In the above implementation, the probability distribution function of the Voronoi cells, $\hat{p}(V_f)$, was evaluated at one hundred equally spaced, discrete values of V_f varying between $V_f = 0$ and $V_f = 1.0$. With the exception of Figs 12 and 13, all computations were performed for $\bar{V}_f = 0.6$. Further details of the numerical schemes are given in the Appendix.

Upon attaining convergence to a prescribed degree of accuracy, the computational program gives the values of v^f, Y, Y' and Y'', as well as the shortening of the column Δ. Results for the non-dimensionalized lateral deflection v^f/L and for the slope Y vs X are shown in Figs 7 and 8 for three values of non-dimensional compressive loads λ, namely $\lambda = 10$, 20 and 26.4. The latter value corresponds to the buckling load, since no equilibrium configuration could be computed for $\lambda > 26.4$. The variation of γ_{xy}^m, the shear strain in the matrix, vs the distance X at $\lambda = 26.4$ is shown by the solid line in Fig. 9. This variation is contrasted with the variation of γ_{xy}^m vs X for uniformly spaced fibers at the same load level, as shown by the dashed line, and against the variation of γ_{xy}^m vs X for uniformly spaced fibers at $\lambda = 29.5$, which is the maximal load level attained in the uniformly spaced case, as shown by the dotted line. All the plots in Fig. 9 correspond to $V_f = 0.6$ (in the case of random spacing $\bar{V}_f = 0.6$ and the results are plotted for the cell with $V_f = 0.6$).

Substitution of the numerically obtained solution for v^f into eqn (6) determines the lateral load $q(x)$ for each Voronoi cell, as specified by its fiber volume fraction V_f. Results for q vs the non-dimensional distance $X = x/L$ are shown in Fig. 10 for a typical "matrix rich" cell, with $V_f = 0.25$, at load levels corresponding to $\lambda = 10$, 20 and the buckling value

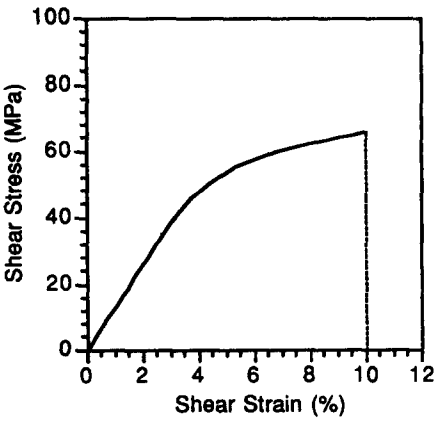

Fig. 6. Shear constitutive relation of PEEK at 21°C based on Guynn's estimation (1992) with shear failure strain assumed at 10%.

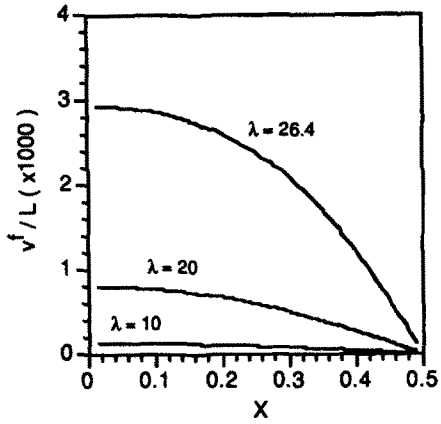

Fig. 7. Non-dimensionalized deflection, v^f/L, vs X for randomly spaced fiber composite with $\bar{V}_f = 0.6$, under compressive loads corresponding to $\lambda = 10$, 20 and 26.4. Failure shear strain γ_u is 10%, and $\lambda = 26.4$ is the compressive strength of the composite.

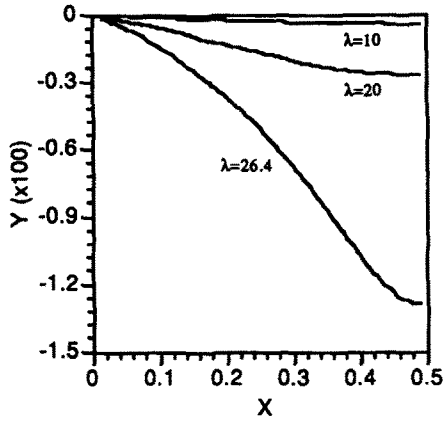

Fig. 8. Solution Y of the governing equation for randomly spaced fiber composite with $\bar{V}_f = 0.6$, under compressive loads corresponding to $\lambda = 10$, 20 and 26.4. Failure shear strain γ_u is 10%, and $\lambda = 26.4$ is the compressive strength of the composite.

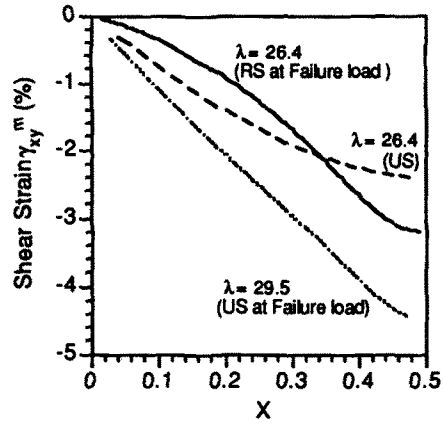

Fig. 9. Comparison between the matrix shear strain within the Voronoi cell with $V_f = 0.6$ in randomly spaced fiber composite under its failure load $\lambda = 26.4$ and the matrix shear strain for uniformly spaced fiber composite under the same load level as well as with its own failure load $\lambda = 29.5$. $\bar{V}_f$ is 0.6 for both cases. RS and US designate randomly and uniformly spaced fiber composite, respectively.

$\lambda = 26.4$. Similar plots are shown in Fig. 11 for a "matrix poor" Voronoi cell, with $V_f = 0.95$. Note that sufficiently low levels of λ, i.e. $\lambda = 10$, yield small values of lateral load q, while increasing levels of λ raise the magnitude of q. It is especially interesting to note

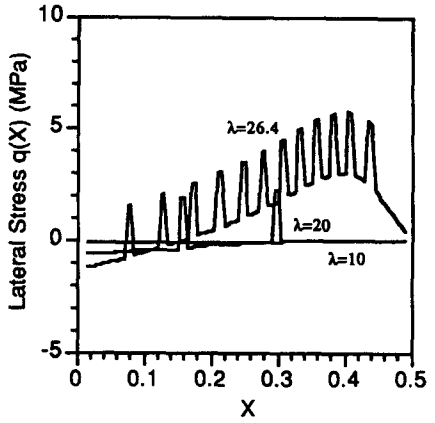

Fig. 10. Lateral stress $q(X)$ vs X on a Voronoi cell with $V_f = 0.25$ in randomly spaced fiber composite with $\bar{V}_f = 0.6$ at various levels of non-dimensional compressive loads λ. The load $\lambda = 26.4$ corresponds to the failure strength of the composite.

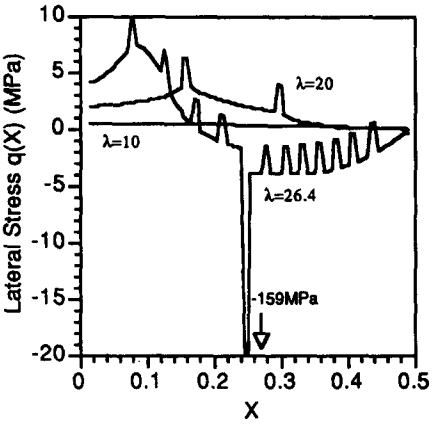

Fig. 11. Lateral stress $q(X)$ vs X on a Voronoi cell with $V_f = 0.95$ in randomly spaced fiber composite with $\bar{V}_f = 0.6$ at various levels of non-dimensional compressive loads λ. The load $\lambda = 26.4$ corresponds to the failure strength of the composite.

the "spikes" in the plots of q vs X. These localized amplifications occur at places where γ_{xy}^m attains its ultimate value γ_u at some Voronoi cells, with the sharpest spike located near the place where $|\gamma_{xy}^m| = \gamma_u$ at the Voronoi cell under consideration. For instance, the spikes in $q(X)$ for $\lambda = 20$ in Fig. 10 occur at $X = 0.15$ and $X = 0.3$, which are the locations where $|\gamma_{xy}^m| = \gamma_u$ at the Voronoi cells of fiber volume fractions $V_f = 0.99$ and $V_f = 0.98$, respectively, at $\lambda = 20$. (Obviously, the matrix material in those cells failed over the ranges of $0.15 < X < 0.5$ and $0.3 < X < 0.5$, respectively.) On the other hand, the sharp spike at $X = 0.25$ for $\lambda = 26.4$ in Fig. 11 is associated with γ_{xy}^m attaining its ultimate value γ_u within the very same Voronoi cell (with $V_f = 0.95$) considered in that figure, while the remaining peaks are associated with shear failures in other cells. Peaks which occur at locations $X < 0.25$ are due to failures in cells with values of $V_f > 0.95$, while spikes located at $X > 0.25$ are due to failures within more resin-rich Voronoi cells.†

Comparison between Figs 10 and 11 shows that resin-rich Voronoi cells are subjected to relatively lower lateral loads. This observation is attributable to the fact that the above mentioned cells sustain shear strains γ_{xy}^m of comparatively smaller magnitudes.

Predicted axial stress–axial strain relations and compressive strengths under monotonically increasing compressive loads are illustrated in Fig. 12 for various values of $\bar{V}_f$. The continuous lines, terminating at points which corresponds to failure, correspond to uniformly spaced fibers, while symbols represent computational results for the case of

† It may seem that lateral equilibrium is not satisfied for the individual Voronoi cells since $\int_0^{1/2} q(X)\,dX \neq 0$ in the plots shown in Figs 10 and 11. However, due to symmetry about $X = 0$ and $X = 0.5$, $\int_0^1 q(X)\,dX$ indeed vanishes.

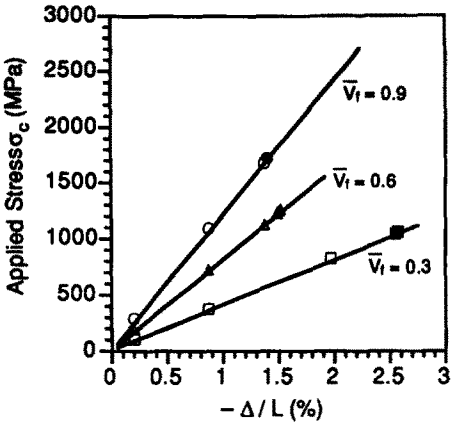

Fig. 12. Dimensionless displacement $-\Delta/L$ at $X = 0.5$ vs applied compressive stress. Solid lines are for uniformly spaced fiber composite. Symbols are for randomly spaced fiber composite. The ends of lines and the filled symbols indicate compressive failure strength for uniform and random spacings, respectively.

randomly spaced Voronoi cells with filled symbols representing failure. The stress–strain responses shown in Fig. 12 are dominated by the last term on the right side of eqn (4) and thus remain nearly linear until failure. In Fig. 13, predicted levels of compressive strength are plotted vs fiber volume fraction, V_f, for uniformly and randomly spaced fibers. Note that random spacings yield lower values of compressive strength and suggest a linear relation between strength and V_f, which is in agreement with experimentally observed trends by Piggott and Harris (1980).

Figures 14(a,b) exhibit plots of fiber curvatures versus non-dimensional distance X at various levels of non-dimensional compressive load λ. Note the significant increase in curvature for the randomly spaced case [Figure 14(b)], as compared with the uniformly spaced case [Figure 14(a)]. If, according to Yin (1992), kinks occur when fibers' curvature attains a critical value, then Figs 14(a,b) suggest that random spacing yield kinks at lower load levels.

Unlike the circumstance of uniformly spaced fibers with bi-linear shear response of the matrix, the computational scheme for randomly spaced fibers cannot be extended to predict post-buckling behavior such as shown in Fig. 2. The specific values of the computed compressive failure stresses are listed in Table 1. Table 1 exhibits the effects of the nominal volume fraction $\bar{V}_f$, the amplitude of geometric imperfection δ_0/L, and the presence or absence of an ultimate value of matrix shear strain γ_u. Table 1 also illuminates the effect of random fiber spacing.

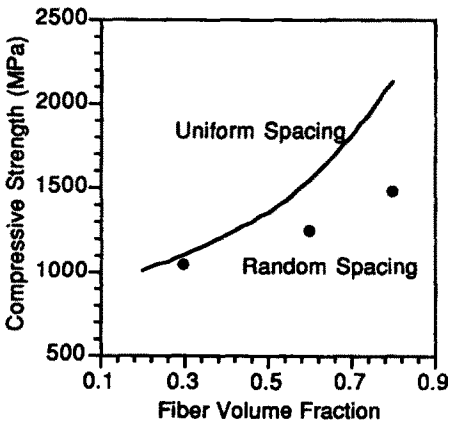

Fig. 13. Compressive strengths of uniformly and randomly spaced fiber composites vs fiber volume fraction.

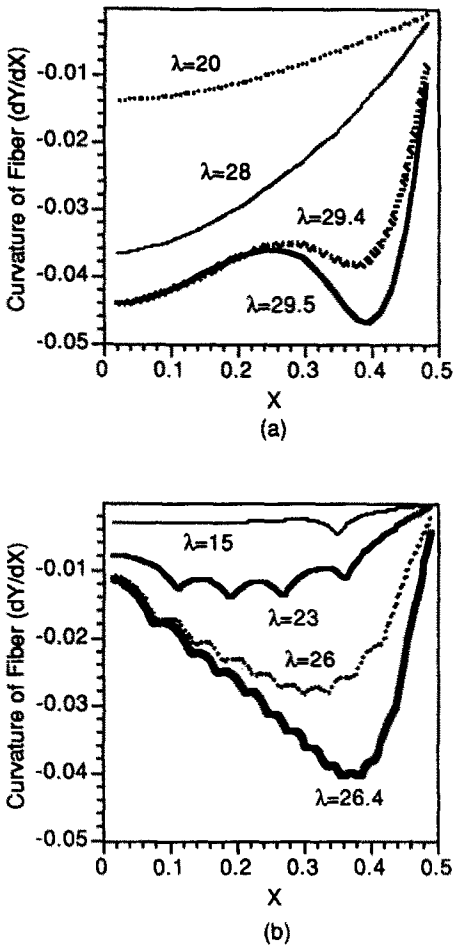

Fig. 14. Pre-buckling curvature of fiber layer in the case of (a) uniformly spaced fiber composite and (b) randomly spaced fiber composite. In both cases $\bar{V}_f = 0.6$.

3. CONCLUDING REMARKS

This article presented a mechanics model for the compressive response and failure of uni-directionally reinforced polymeric composites loaded parallel to the fiber direction. The model accounted for the non-linear shear response of the resin, including its ultimate shear strain, and incorporated two kinds of geometric imperfections, namely, initial fiber waviness and random fiber spacings. Heretofore, the latter kind of imperfection has not been considered elsewhere.

The non-linear response of the matrix was accounted for by means of the non-linear field eqn (6) for the lateral displacement v^f. In general, the above equation could be solved

Table 1. Comparison of failure strength (MPa)

$\bar{V}_f$	δ_0/L	Uniform spacing $\gamma_u = \infty$	Uniform spacing $\gamma_u = 0.1$	Random spacing $\gamma_u = \infty$	Random spacing $\gamma_u = 0.1$
0.3	0.0025	1360	1360	1381	1292
	0.0050	1103	1103	1116	1029
	0.0075	941	941	947	867
0.6	0.0025	2023	2023	2144	1746
	0.0050	1541	1541	1583	1234
	0.0075	1253	1253	1281	969
0.9	0.0025	4228	4228	4228	2927
	0.0050	2702	2702	2685	1700
	0.0075	2023	2023	2023	1194

numerically up to failure. Nevertheless, in some special circumstances, it was possible to generate a solution into the post-buckling range.

Both kinds of geometric imperfections, initial fiber waviness and random fiber spacings, were shown to substantially reduce the compressive strength of the composite. However, random fiber spacings, when combined with the foregoing non-linear shear response of the matrix, was shown to introduce imbalances in the support furnished by the matrix against fiber micro-buckling, resulting in highly localized internal transverse loads on the fibers. The emergence of these transverse loads alludes to the possibility of transition from micro-buckling to micro-kinking of the deformed fibers. However, it is impossible to explore this matter any further within the context of the Bernoulli–Euler beam theory utilized in the present article since this theory cannot account for discontinuous shear deformations within the fibers. Such discontinuities are likely to occur at locations where the matrix reaches its ultimate strength and ceases to support the fibers, and the highly concentrated transverse loads predicted by the present analysis reflect the indeterminacy inherent in the Bernoulli–Euler theory in addressing shear response.

A remedy to the above inadequacy may be found by employing shear-deformation models, such as the Timoshenko beam theory, to represent the response of the fibers. This approach was employed recently by Chung and Weitsman (1993), where it was shown that random fiber spacing indeed causes discontinuities in the shear strains within the fibers. These discontinuities indicate the emergence of kinks.

Acknowledgment—This work was performed under Contract N00014-90-J-1556 from the Office of Naval Research to one of the authors (YW). The authors wish to thank the program manager, Dr. Y. Rajapakse of the Mechanics Division, Engineering Sciences Directorate, for his encouragement and support.

REFERENCES

Blake, H. W. and Starbuck, J. M. (1993). Hydrostatic testing of thick laminated composite cylinders for performance model validation. *Report ORNL/ATD-67*. Oak Ridge National Laboratory, TN.

Budiansky, B. and Fleck, N. A. (1992). Compressive failure of fibre composites. *J. Mech. Physics Solids* **41,** 193–211.

Camponeschi, Jr, E. T. (1991). Compression of composite materials: a review. *Composite Materials: Fatigue and Fracture, ASTM STP 1110*, pp. 550–578.

Chung, I. and Weitsman, Y. J. (1993). A model for the micro-buckling/micro-kinking compressive response of fiber-reinforced composites. To appear in *Proc. 12th U.S. National Conference of Applied Mechanics*. Seattle, WA.

Davis, Jr, J. G. (1975). Compressive strength of fiber-reinforced composite materials. *Composite Reliability, ASTM STP 580*, pp. 364–377.

Davy, P. J. and Guild, F. J. (1988). The distribution of interparticle distance and its application in finite element modeling of composite materials. *Proc. R. Soc. London* **A418,** 95–112.

Evans, A. G. and Adler, W. F. (1978). Kinking as a mode of structural degradation in carbon fiber composites. *Acta Metall.* **26,** 725–738.

Garg, S. K., Svalbonas, V. and Gurtman, G. A. (1973). *Analysis of Structural Composite Materials*. Dekker, New York.

Greszczuk, L. B. (1975). Microbuckling failure of circular fiber-reinforced composites. *AIAA J.* **13,** 1311–1318.

Guynn, E. G., Ochoa, O. O. and Bradley, W. L. (1992). A parametric study of variables that affect fiber microbuckling initiation in composite laminates: part 1 analyses. *J. Composite Mater.* **26,** 1594–1616.

Hahn, H. T. and Williams, J. G. (1986). Compression failure mechanisms in unidirectional composites. *Composite Materials: Testing and Design, ASTM STP 893*, pp. 115–139.

Hermann, L. R., Mason, W. E. and Chan, S. T. K. (1967). Response of reinforcing wires to compressive states of stress. *J. Composite Mater.* **1,** 212–226.

Highsmith, A. L., Davis, J. I. and Helms, K. L. E. (1992). The influence of fiber waviness on the compressive behavior of unidirectional continuous fiber composites. *Composite Materials: Testing and Design, ASTM STP 1120*, pp. 20–36.

Johnston, N. J., Towell, T. W. and Hergenrother, P. M. (1991). Physical and mechanical properties of high performance thermoplastic polymers and their composites. In *Thermoplastic Composite Materials* (Edited by L. A. Carlsson), pp. 27–71. Elsevier Science, Amsterdam.

Lanir, Y. and Fung, Y. C. B. (1972). Fiber composite columns under compression. *J. Composite Mater.* **6,** 387–401.

Lin, K. Y. and Zhang, X. J. (1992). Effect of fiber waviness on the compressive strength of laminated composites. *Proc. 2nd Int. Symposium on Composite Materials and Structures*, pp. 120–125. Beijing, China.

Morley, J. G. (1987). *High Performance Fiber Composites*. Academic Press.

Na, T. Y. (1979). *Computational Methods in Engineering Boundary Value Problems*. Academic Press.

Piggott, M. R. (1993). Compressive strength of composites: how to measure it and how to improve it. *Proc. Int. Conference on Advanced Composite Materials*, pp. 51–59. Wollongong, Australia, February 15–19, 1993.

Piggott, M. R. and Harris, B. (1980). Compression strength of carbon, glass and Kevlar-49 fibre reinforced polyester resins. *J. Mater. Sci.* **15,** 2523–2538.
Rosen, B. W. (1965) Mechanics of composite strengthening. *Fiber Composite Materials, American Society for Metals*, pp. 37–75.
Sadowsky, M. A., Pu, S. L. and Hussain, M. A. (1967). Buckling of microfibers. *J. Appl. Mech.* **34,** 1011–1016.
Shuart, M. J. (1985). Short-wavelength buckling and shear failures for compression-loaded composite laminates. *NASA TM 87640.*
Shuart, M. J. (1989). Failure of compression loaded multidirectional composite laminates. *AIAA J.* **27,** 1274–1279.
Simitses, G. J. (1976). *An Introduction to the Elastic Stability of Structures.* Prentice-Hall, NJ.
Steif, P. S. (1988). A simple model for the compressive failure of weakly bonded fiber reinforced composites. *J. Composite Mater.* **22,** 818–828.
Wang, A. S. D. (1978). A nonlinear microbuckling model predicting the compressive strength of unidirectional composites. *ASME Paper 78-WA/Aero-1*, pp. 1–8.
Yin, W. L. (1992). A new theory of kink band formation. *AIAA-92-2552-CP*, pp. 3028–3035.

APPENDIX: THE NUMERICAL SCHEME

The non-linear second order differential eqn (13) can be expressed as

$$Y'' = Q(X, Y) \tag{A1}$$

where the prime denotes derivatives with respect to X, and

$$Q(X, Y) = \int_0^1 \hat{p}(V_f)\alpha^2(V_f)(1-V_f)F\left(\frac{Y}{1-V_f}\right)\mathrm{d}V_f - \lambda^2 Y - \lambda^2 Y_0.$$

An error quantity at ith iteration step is defined as

$$\phi^{(i)} = Y''^{(i)} - Q(X, Y^{(i)}).$$

Consequently, upon employing a Taylor series expansion, the subsequent error quantity is given by

$$\phi^{(i+1)} = \phi^{(i)} + \left(\frac{\partial\phi}{\partial Y}\right)^{(i)}(Y^{(i+1)} - Y^{(i)}) + \left(\frac{\partial\phi}{\partial Y''}\right)^{(i)}(Y''^{(i+1)} - Y''^{(i)}). \tag{A2}$$

Noting that

$$\left(\frac{\partial\phi}{\partial Y}\right)^{(i)} = -\left(\frac{\partial Q}{\partial Y}\right)^{(i)} \quad \text{and} \quad \left(\frac{\partial\phi}{\partial Y''}\right)^{(i)} = 1,$$

we obtain, upon imposing $\phi^{(i)} = \phi^{(i+1)} = 0$ in eqn (A2),

$$Y''^{(i+1)} - \left(\frac{\partial Q}{\partial Y}\right)^{(i)} Y^{(i+1)} = Q(X, Y^{(i)}) - \left(\frac{\partial Q}{\partial Y}\right)^{(i)} Y^{(i)}. \tag{A3}$$

Expression (A3) is a linear ordinary differential equation for $Y^{(i+1)}$ involving the known results of the previous iteration $Y^{(i)}$. Note that the derivative of Q with respect to Y is

$$\frac{\partial Q}{\partial Y} = \int_0^1 \hat{p}(V_f)\alpha^2(V_f)F'\left(\frac{Y}{1-V_f}\right)\mathrm{d}V_f - \lambda^2.$$

Furthermore, upon employment of the Ramberg–Osgood model, we have

$$F' = \frac{1}{1 + \dfrac{G_e^m}{A^{1/n}n}(\tau_{xy}^m)^{(1-n)/n}}.$$

Obviously, the boundary conditions in eqn (15) must be satisfied in every iteration step.

The linear differential eqn (A3) is solved by a finite difference scheme as follows. Divide the abscissa $0 < X < 1$ into N equal intervals of length $h = 1/N$. Then at each node, $X = X_n = nh$, the second derivative Y'' is expressed as

$$Y_n'' = \frac{1}{h^2}(Y_{n+1} - 2Y_n + Y_{n-1}).$$

Using the above relation, eqn (A3) can be converted to an algebraic equation of the form

$$Y_{n-1}^{(i+1)} + b_n^{(i+1)} Y_n^{(i+1)} + Y_{n+1}^{(i+1)} = r_n^{(i+1)}. \tag{A4}$$

Here,

$$b_n^{(i+1)} = -h^2 \left(\frac{\partial Q}{\partial Y}\right)_n^{(i)} - 2$$

$$r_n^{(i+1)} = h^2 \left\{ Q(X_n, Y_n^{(i)}) - \left(\frac{\partial Q}{\partial Y}\right)_n^{(i)} Y_n^{(i)} \right\}.$$

The boundary conditions in finite difference scheme are $Y_0^{(i+1)} = 0$ and $Y_{N+1}^{(i+1)} = Y_{N-1}^{(i+1)}$.

The system of eqns (A4) can be represented as

$$\mathbf{A}^{(i+1)} \mathbf{Y}^{(i+1)} = \mathbf{S}^{(i+1)}, \tag{A5}$$

where

$$\mathbf{A}^{(i+1)} = \begin{bmatrix} b_1^{(i+1)} & 1 & & & & 0 \\ 1 & b_2^{(i+1)} & 1 & & & \\ & 1 & b_3^{(i+1)} & 1 & & \\ & & & \ddots & & \\ & & & 1 & b_{N-1}^{(i+1)} & 1 \\ 0 & & & & 2 & b_N^{(i+1)} \end{bmatrix}, \quad \mathbf{Y}^{(i+1)} = \begin{Bmatrix} Y_1^{(i+1)} \\ Y_2^{(i+1)} \\ \vdots \\ Y_N^{(i+1)} \end{Bmatrix}, \quad \mathbf{S}^{(i+1)} = \begin{Bmatrix} r_1^{(i+1)} \\ r_2^{(i+1)} \\ \vdots \\ r_N^{(i+1)} \end{Bmatrix}.$$

Equation (A5) can be solved by means of the LU decomposition (Na, 1979). Accordingly, the matrix $\mathbf{A}^{(i+1)}$ is decomposed into the product $\mathbf{A}^{(i+1)} = \mathbf{L}^{(i+1)}\mathbf{U}^{(i+1)}$. Here,

$$\mathbf{L}^{(i+1)} = \begin{bmatrix} \beta_1^{(i+1)} & & & & 0 \\ 1 & \beta_2^{(i+1)} & & & \\ & \ddots & & & \\ & & 1 & \beta_{N-1}^{(i+1)} & \\ 0 & & & 2 & \beta_N^{(i+1)} \end{bmatrix}, \quad \mathbf{U}^{(i+1)} = \begin{bmatrix} 1 & \gamma_1^{(i+1)} & & & 0 \\ & 1 & \gamma_2^{(i+1)} & & \\ & & \ddots & & \\ & & & 1 & \gamma_{N-1}^{(i+1)} \\ 0 & & & & 1 \end{bmatrix}$$

and

$$\beta_1^{(i+1)} = b_1^{(i+1)}$$

$$\beta_n^{(i+1)} \gamma_n^{(i+1)} = 1 \quad (n = 1, 2 \ldots N-1)$$

$$\beta_n^{(i+1)} = b_n^{(i+1)} - \gamma_{n-1}^{(i+1} \quad (n = 2, 3 \ldots N-1)$$

$$\beta_N^{(i+1)} = b_N^{(i+1)} - 2\gamma_{N-1}^{(i+1)}.$$

Denoting

$$\mathbf{Z}^{(i+1)} = \mathbf{U}^{(i+1)} \mathbf{Y}^{(i+1)}, \tag{A6}$$

eqn (A5) is transformed to $\mathbf{L}^{(i+1)}\mathbf{Z}^{(i+1)} = \mathbf{S}^{(i+1)}$, where the components of $\mathbf{Z}^{(i+1)}$ are computed by

$$z_1^{(i+1)} = r_1^{(i+1)} / \beta_1^{(i+1)}$$

$$z_n^{(i+1)} = (r_n^{(i+1)} - z_{n-1}^{(i+1)}) / \beta_n^{(i+1)} \quad (n = 2, 3 \ldots N-1)$$

$$z_N^{(i+1)} = (r_N^{(i+1)} - 2z_{N-1}^{(i+1)}) / \beta_N^{(i+1)}.$$

The recursive relations between $z_n^{(i+1)}$ and $Y_n^{(i+1)}$ are obtained from eqn (A6) as

$$Y_N^{(i+1)} = z_N^{(i+1)}$$

$$Y_n^{(i+1)} = z_n^{(i+1)} - \gamma_n^{(i+1)} Y_{n+1}^{(i+1)} \quad (n = N-1, N-2 \ldots 1).$$

The values of $Y_n^{(i+1)}$ express the solution to eqn (13) at the $(i+1)$th iterative step. When

$$\sum_{n=1}^{N} |Y_n^{(i+1)} - Y_n^{(i)}|^2$$

attains a constant value within a prescribed tolerance, the iteration is halted and post-processed to compute deflection, shear strain and stress, lateral stress and other quantities.